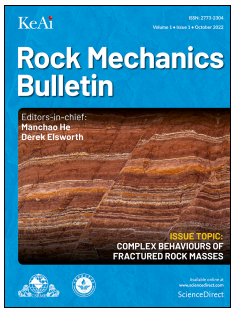

Deep Learning-Powered Rock Mass Classification: Predicting RMR from Q-System Parameters with High Accuracy

Tawanda Zvarivadza, Abiodun Ismail Lawal, Moshood Onifade, Francois Mulenga, Sangki Kwon, Manoj Khandelwal

PII: S2773-2304(25)00046-0

DOI: https://doi.org/10.1016/j.rockmb.2025.100219

Reference: ROCKMB 100219

To appear in: *Rock Mechanics Bulletin*

Received Date: 24 March 2025

Revised Date: 12 May 2025

Accepted Date: 25 May 2025

Please cite this article as: Zvarivadza, T., Lawal, A.I., Onifade, M., Mulenga, F., Kwon, S., Khandelwal, M., Deep Learning-Powered Rock Mass Classification: Predicting RMR from Q-System Parameters with High Accuracy, *Rock Mechanics Bulletin*, https://doi.org/10.1016/j.rockmb.2025.100219.

Deep Learning-Powered Rock Mass Classification: Predicting RMR from Q-System Parameters with High Accuracy

Tawanda Zvarivadza[1], Abiodun Ismail Lawal[2], Moshood Onifade[3], Francois Mulenga[2], Sangki Kwon[4], Manoj Khandelwal[3*]

[1]Department of Civil, Environmental and Natural Resources Engineering, Luleå University of Technology, Luleå, Sweden

[2]Department of Mining Engineering, University of South Africa, Florida Campus Private Bag X6, Johannesburg 1710, South Africa

[3]Institute of Innovation, Science and Sustainability, Federation University Australia, Ballarat, Victoria 3350, Australia

[4]Department of Energy Resources Engineering, Inha University, Yong-Hyun Dong, Nam Ku, Incheon, South Korea

Abstract

Reliable stability assessment requires an objective and precise assessment of the rock mass quality classification. A deep learning model is developed to create a tool that can provide a rapid and precise assessment of the quality of rock masses. While there are empirical equations to determine RMR values from Q parameters, this study provides an advanced highly accurate deep learning approach to determine RMR values from Q parameters. This serves to reduce the amount of fieldwork related to collecting the rockmass data needed to independently assess rockmass quality using the RMR system and the Q system separately. The RMR values, like Q values, were first determined independently in the field. The deep learning approach was later used to predict the field-determined RMR values from the field-determined Q parameters. This means that each practical field measurement point had an RMR, and a Q value independently determined for it before the deep learning approach was applied. The six rockmass parameters of the Q system (RQD, J_n, J_r, J_a, J_w, SRF) are used as input in this model while the RMR is used as the output variable. In this study, the dataset contains 356 samples, 70%, 15% and 15% of the entire sample data are used to train, test, and validate the model, respectively. The predictive performance of the models was evaluated and compared using metrics such as R^2, MAE, and RMSE among many others. The overall R^2 values for the ANN, FDA-ANN and SCA-ANN are 0.9951, 0.996 and 0.9955 respectively. The MAE values are 0.099, 0.096 and 0.085 for ANN, FDA-ANN and SCA-ANN respectively. The FDA-ANN model has a higher accuracy than other techniques, such as the ANN and SCA-ANN. The error values obtained for each of the models are very close to their expected value of 0 while their obtained R^2 and VAF are also much closer to the targeted value of 1 and 100% respectively. The PI is also close to the expected value of 2. Hence, the three proposed models can be confidently used in predicting RMR values using Q parameters obtained from field investigations without the need to independently determine RMR from the traditional RMR field parameters. The study used the Chord diagram to display the rank of the performance indicators and the sensitivity analysis using the Cosine Amplitude methods (CAM). It shows that the RQD parameter has the highest CAM value followed by J_w and then J_n for all three models. The results offered here provide insight for engineers and academics who are interested in analysing rock mass classification criteria or conducting field investigations.

Keywords: Deep learning; Rock Mass Rating (RMR); Q parameters; Neural network; ANN

1 Introduction

The development of underground structures has a lengthy history. Underground engineering was primarily done by experience in the past because of the lack of knowledge of the characteristics of rock and soil (Spross et al., 2019). Historical cases and the geotechnical situation are heavily depended upon and have been used as reference models for projects that have come after (Bieniawski, 1989). Under these circumstances, techniques for classifying rocks are created as guidelines for assessing excavation activities and the support needs of subsurface structures. Established nearly 50 years ago, the rock mass rating system was initially introduced by Bieniawski (1973). It was first established to estimate the amount of support needed during tunnel excavation. Based on case studies, RMR has undergone numerous modifications over the years. Eight characteristics are considered for classifying a jointed rock mass in the 1973 version of the RMR system. There are five rating stages for each parameter. The first RMR version, according to Aksoy (2008), attempts to assess the stability of an unsupported tunnel segment in weak rock that is exposed to water. Large ground deformation during tunnel excavation may happen in a soft rock area, endangering the construction site's safety. RMR can be used to assess the unsupported underground opening's stable period. This allows for the proper management of risk and the assessment of the approximate maximum span between the tunnel face and a supported section.

In general, stability analysis in rock engineering requires the assessment of rock mass quality. Numerous techniques for classifying rock masses have been developed by academics. According to their observed structure and hardness, rock mass was divided into nine groups in Terzaghi's (1946) rock load theory. The rock quality designation (RQD), developed by Deere in 1963, uses drill core log observation to objectively determine the quality of rock mass. Numerous geoengineering projects have made substantial use of this approach, which has gained widespread acceptance (Zhang et al., 2013; Zhu et al., 2011). Naturally, the RQD approach cannot fully capture the comprehensive influence of rock mass structures, hydrogeological factors, and several other elements because it is a single-index classification method. The rock mass rating (RMR) system was proposed by Bieniawski (1973) using case studies from civil engineering that were accessible. Additionally, it provides us with a helpful guide when figuring out the parameters that influence rock mass.

A new method for classifying rock masses has been made possible by the advancement of machine learning (ML). New advancements in rock mass engineering are brought about by the development of artificial intelligence technologies (Bao et al., 2025; Zhang and Phoon, 2022; Hussain et al., 2016). Azarafza et al. (2020) used artificial intelligence methods such as support vector machines and k-nearest neighbours to figure out the altered relationship between slope stability and Q-slope. A convolutional neural network (CNN) was developed by Wang et al. (2020) to carry out rock slope recognition. Additionally, Chen et al. (2021) offered a CNN-based paradigm for categorizing rock formations. Slope stability (Zhang et al., 2022), joint recognition (Liu et al., 2025; Fathipour-Azar, 2021), rock mass prediction and classification (Gholami et al., 2013; Chen et al., 2022), tunnel boring machine (TBM) and tunnel parameter optimisation (Hou et al., 2022; Wu et al., 2021) are a few of the geotechnical fields that have benefited from the application of deep learning, digital image technology, and machine learning technologies. Among these, deep learning algorithms are at the heart of numerous technologies that are advancing the realisation of intelligence across a range of domains. To develop the intricate mapping link between the original data and the target, it is frequently used to thoroughly mine the features of the original data, including digital images, radar point clouds, speech, and audio.

CNNs (Lawrence et al., 1997), recurrent neural networks (Hochreiter and Schmidhuber, 1997), deep belief networks (Le Roux and Bengio, 2008; Niu et al., 2024), autoencoders (Gao et al., 2020, Sheng et al., 2023), and other models have been proposed for deep learning (Narimani et al., 2025; Liu et al., 2024). Civil engineering has made extensive use of neural networks (Adeli, 2001). Deep neural networks (DNNs) are created as neural network technology advances. To determine the RQD value in geotechnical engineering, Liu et al. (2021) automatically identified a single row of cores from the drill core image using the mask region-CNN (RCNN). They then utilised standard Kriging interpolation to create a block model that could describe the heterogeneity of RQD by combining the drill data with the theoretical geological model. He et al. (2021) used a deep CNN model to continuously predict the rock strength parameters based on the drilling data. A novel approach based on DNN and spectrogram analysis was presented by Han et al. (2019) for the non-destructive measurement of rock surface strength. Wu et al. (2019) integrated Monte Carlo simulation (MCS) and the order preference by similarity to the ideal solution (TOPSIS) technique, considered the impact of parameter uncertainty and suggested a novel approach to classify the quality of rock mass. Sheng et al. (2023) used the stacked autoencoders (SAE) deep learning model to predict the rock mass classification objectively and efficiently. Their suggested method has a higher accuracy than other deep learning techniques, such as ANN and RBF, and was validated using a typical rock slope in Changsha, China. The findings demonstrate that the SAEs accurately classify every test sample, while the confusion matrix is used to calculate the ANN and RBF rating accuracies, which are 97.5% and 98.7%, respectively.

1.1 Review of some approaches used to estimate or predict RMR

The RMR classification system is one of the most well-known and often utilised rock mass classification techniques in tunnel design, mine support systems, and stability analysis today. Because of the anisotropic nature of the rock mass and the nonlinear relationships between the RMR parameters, assessing the rock mass using RMR is quite difficult. Multiple linear regression and ANN-based models are examples of artificial intelligence that are used to address nonlinear relations issues in engineering. They may also be used to validate and enhance design solutions in any engineering project. Empirical equations can be used to predict RMR values from Q parameters (see Eq. (1) (Bieniawski, 1976) and Eq. (2) (Choquet and Hadjigeorgiou, 1993)).

$$\mathrm{RMR} = 9\ln Q + 44 \tag{1}$$

$$\mathrm{RMR} = 5\ln Q + 60.8 \tag{2}$$

A thorough field investigation done by Zvarivadza (2012) showed that the accuracy of these equations varies depending on the rockmass analysed. Existing empirical equations can convert Q-system parameters into RMR values, yet they often rely on multiple steps or assumptions that can introduce uncertainty and increase data collection demands in the field. Table 1 is a comprehensive table presenting some of the various approaches for predicting and determining RMR. The table covers both classical and modern data-driven methods for determining RMR. Each approach offers unique benefits for specific site conditions and project demands, emphasising a balance between data availability, computational complexity, and interpretability.

Table 1. Reflection on some classical and modern data-driven RMR determination methods

References	Method used	Strengths	Limitations
Bieniawski (1973, 1989)	Original RMR classification	Widely used and recognised baseline for rock mass classification. Straightforward parameter-based approach.	Subjective parameter rating. Limited ability to capture complex or highly variable conditions.
Romana (1985)	Slope Mass Rating (SMR) based on RMR	Adaptation of RMR for slope stability. Considers joint orientation corrections.	Requires site-specific slope geometry data. Additional correction factors introduce complexity.
Abbas et al. (2024)	Correlation of RMR with Q-System	Facilitates cross-comparison between Q and RMR. Supports integrated use of multiple classification systems.	Correlations may not hold in all geological settings. Potential misalignment of input parameter definitions.
Nejati et al. (2014)	RMR modifications for rock mass deformability	Emphasises deformability aspects of rock mass. Suitable for large underground openings.	Requires extensive lab testing (E-modulus, Poisson's ratio). Still partly relies on conventional RMR ratings.
Rezaei and Habibi (2023)	Empirical correlations (RMR vs. stand-up time)	Directly links RMR with tunnel stability durations. Useful for preliminary support design.	Highly empirical and site-specific. May oversimplify complex ground conditions.
Serafim and Pereira (1983)	RMR Hoek-Brown correlation	Provides a relationship between RMR and the Hoek-Brown failure criterion. Widely used in numerical analysis.	Based on limited datasets. Potentially inaccurate for weathered or altered rock.
Hoek, Kaiser and Bawden (2000)	GSI System correlated to RMR	GSI (Geological Strength Index) offers a simpler field estimation than standard RMR. Reduces reliance on lab UCS testing	Subjectivity in GSI window selection. Approximate correlations to the original RMR table.
Soufi et al. (2018)	Empirical correlation between RMR, Q, and other systems	Cross-checks consistency among multiple classification indices. Provides simpler conversions in data-scarce conditions.	Regression-based, so less reliable beyond the original calibration range. Potential mismatch in parameter definitions among classification systems.
Stille and Palmström (2003)	RMR correlation with Rock Mass Index (RMi)	Integrates block size and joint shear strength. Potentially better representation of blocky rock masses.	Requires thorough identification of joint characteristics. Additional complexity vs. original RMR.
Jalalifar et al. (2014)	Fuzzy logic approach to RMR prediction	Deals with vagueness and uncertainty in rock mass parameters. More flexible than strict numeric thresholds.	Requires rigorous definition of fuzzy sets and rules. Can be subjective in membership function design.
Mert, Yilmaz and İnal (2011)	Neural Network modeling for RMR	Captures nonlinear interactions among parameters. Automates rating predictions given training data.	Requires large, high-quality datasets. Risk of overfitting if not properly validated.
Sadrossadat et al. 2018	ANFIS (Adaptive Neuro-Fuzzy Inference System) for RMR	Combines neural nets and fuzzy logic to handle uncertainty. Potentially higher accuracy in parameter weighting.	Complex architecture setup. Computationally demanding, especially for large datasets.
Salimi et al. (2018)	Genetic Programming (GP) to predict RMR	Learns underlying relationships to produce explicit formulae. Good at handling complex parameter interactions.	Formulas can be difficult to interpret physically. Overfitting risk without proper cross-validation.
Li et al. (2024)	Bayesian approach to RMR parameter updating	Systematic incorporation of new data (e.g., in tunnel face mapping). Quantifies parameter uncertainty and reliability.	More complex computations. Requires well-defined priors and significant field data.

References	Method used	Strengths	Limitations
Hu et al. (2022)	SVM (Support Vector Machine) for RMR prediction	Good generalisation with fewer data points relative to ANN. Efficient at handling high-dimensional input.	Requires kernel parameter tuning. May be less intuitive to interpret than rule-based or regression models.
Santos et al. (2022)	Random Forest regression for RMR	Aggregates multiple decision trees, reducing variance. Provides feature importance for parameter weighting.	Less transparent than linear models. Can require substantial computational resources for large ensembles.
Wu and Wang (2024)	Extreme Learning Machine (ELM) for RMR	Fast training times compared to classic ANN. Good performance on moderate to large datasets.	Limited acceptance vs. mainstream machine learning methods. Potential sensitivity to random weight initialisation.
Sari, Karpuz and Ayday (2010)	Probabilistic RMR approach with Markov processes	Accounts for spatial variability along tunnel length. Dynamic updating as excavation progresses.	Requires advanced stochastic modelling expertise. Can be computationally intensive.
Saadati et al. (2024)	Multi-criteria approach integrating RMR and field data	Balances both laboratory and field observations. Considers multiple rating factors in a single framework.	Complexity in weighting or scoring can be subjective. Requires expert involvement.
Peng et al. (2022)	Analytical Hierarchy Process (AHP) integrated with RMR	Structured pairwise comparison of influencing parameters. Can incorporate expert judgment systematically.	Subjectivity in pairwise comparisons. Risk of inconsistency in large or multi-expert contexts.
Armaghani et al. (2017)	Hybrid ANN-PSO for RMR determination	Particle Swarm Optimisation (PSO) optimises ANN hyperparameters. Potentially improves convergence speed and global search.	Requires swarm parameter tuning. Computational overhead may be high.
Chen et al. (2024)	Discrete Fracture Network (DFN) to refine RMR assumptions	Captures detailed fracture geometry beyond simple spacing. Better at modelling realistic joint networks.	Data-heavy approach (detailed 3D mapping needed). Model complexity can be high, making it harder to implement.
Jin et al. (2023)	MCS + TOPSIS multi-criteria for RMR classification	Incorporates uncertainty quantification via Monte Carlo Simulation. Ranks multiple influencing factors systematically (TOPSIS).	Requires careful weighting of parameters in TOPSIS. Computational overhead for MCS can be significant.

Bieniawski's (1989) RMR: The foundational rating system for rock mass characterisation, assessing factors such as UCS, RQD, spacing, condition of discontinuities, groundwater, and adjustment for discontinuity orientation.

Empirical correlations and hybrid methods: Many approaches blend or compare RMR with other systems (Q, GSI, RMi) or apply statistical correlations.

Machine learning and intelligent systems: Neural networks, SVMs, genetic algorithms, and hybrid swarm-ANN methods can uncover complex nonlinear relationships if sufficient high-quality data is available. Interpretability and overfitting, however, remain key concerns.

Multi-criteria decision methods (e.g., TOPSIS, AHP): Incorporate expert judgment and advanced ranking frameworks to refine RMR or combine it with additional parameters.

Probabilistic and stochastic approaches: Bayesian methods, Markov chains, and Monte Carlo simulations address inherent uncertainty but can be more complex to implement.

1.2 Current study and its novelty robustness

The method presented in this study capitalises on an advanced deep learning architecture to directly forecast RMR from the six fundamental Q-system parameters—Rock Quality Designation (RQD), Joint Set Number (J_n), Joint Roughness Number (J_r), Joint Alteration Number (J_a), Joint Water Reduction Factor (J_w), and Stress Reduction Factor (SRF). The deep learning model leverages these six parameters as input features to automatically capture complex interdependencies that traditional correlation equations might oversimplify. In this study, it is crucial to note that both RMR and Q values were originally determined through independent field measurements, ensuring that each data point reflects genuine geological

conditions prior to any modeling. RMR determination, for example, typically involves an array of rock mass attributes such as uniaxial compressive strength and condition of discontinuities. Parallel to this process, the Q-system parameters were measured in the same localities to create a comprehensive dataset. Once these values were paired, the deep learning model was trained to map from Q-based indicators to the observed RMR ratings. Using this approach, the requirement to compile entirely separate datasets for each classification system can be reduced. Field practitioners, therefore, benefit from faster and more focused data-gathering procedures, since Q parameters alone can now support estimates of RMR with high accuracy. This approach significantly streamlines rock mass characterisation in situations where time, budget, or operational constraints may limit extensive field campaigns. The inherent variability of rock mass conditions is more effectively addressed by deploying a deep learning strategy as these models have the capacity to learn complex, nonlinear relationships within the dataset. The predictive power gained from this practical, tethered in reality, study translates to a more dependable tool for informing engineering decisions. The developed deep learning technique stands as a promising alternative for practitioners seeking to integrate two major classification frameworks (RMR and Q) without duplicating the laborious fieldwork often associated with separate systems.

This study simulated several ANN models with single-hidden layers and double-hidden layers. The best among the simulated ANN models is subjected to novel flow direction and sine-cosine optimisation algorithms. The dataset contains 356 samples with Q-system parameters (RQD, J_n, J_r, J_a, J_w, SRF) used as input in this model while the RMR is used as the output variable. The predictive performance of the models was evaluated and compared using metrics such as R^2, MAE, and RMSE among many others. The optimal RMR prediction model was then determined, and the Chord diagram was used to score rank the models. The contributions of this study are that (a) the novel FDA and SCA-optimised ANN model is used to make very accurate and objective predictions about the RMR from the Q-system input parameters; (b) the FDA-ANN model has higher accuracy than other techniques, such as ANN and SCA-ANN, (c) the use of Chord diagram to display the rank of the performance indicators and (d) the influence of parameters RQD and J_w is more pronounced on RMR.

2 Geological context and economic significance of the Great Dyke of Zimbabwe

The Great Dyke of Zimbabwe (Fig. 1) is a prominent linear geological feature that extends roughly 550 km along a northeast-southwest axis, traversing much of the central region of the country. Formed approximately 2.5 billion years ago during the Precambrian, it stands as a classic example of a layered mafic and ultramafic intrusion. This elongated structure, which generally measures between 4 and 11 km in width, showcases pronounced layering reflective of distinct mineral deposition events. Magma once intruded the host rock and cooled in successive stages, giving rise to well-defined layers composed predominantly of gabbro, norite, dunite, and pyroxenite. The Great Dyke is geologically divided into four principal complexes –Musengezi, Hartley, Selukwe, and Wedza – each distinguished by its own mineralogical and structural complexities. These segments reveal variations in the proportion of mafic to ultramafic rocks, the thickness of igneous layers, and the abundance of specific mineral deposits. One of the standout features of the Dyke is its chromitite layers, which contain especially high concentrations of chromium. This chromium endowment has positioned the Great Dyke as one of the world's most significant chromium repositories, ensuring its ongoing importance in stainless steel production and related industries. The Dyke hosts a diverse suite of minerals that further enhance its economic and geological value beyond chromium. Platinum group metals (PGMs) such as platinum, palladium, and rhodium—critical for catalytic

converters and various high-tech applications–are present, often in association with nickel, copper, and lesser amounts of gold. These minerals are typically dispersed within pyroxenitic or gabbroic layers, necessitating specialised methods to target and extract them efficiently. Given their global demand, these PGMs and associated base metals underscore the strategic importance of the Dyke for the mining sector of Zimbabwe. From a structural perspective, the elongated, ribbon-like shape of the Great Dyke is a product of the initial magmatic intrusion and subsequent tectonic forces that influenced its final form. The interplay of cooling rates, mineral crystallization sequences, and local tectonic stresses resulted in the layered pattern now observed in outcrops and active mine faces. This unique structure not only fascinates geologists but also challenges mining practitioners who must adapt their extraction methods to complex rock mass conditions. In economic terms, the Great Dyke is a cornerstone of Zimbabwe's minerals industry. The extraction of chromite and PGMs contributes substantially to both export revenues and local employment. Secondary or by-product minerals—such as nickel and copper—further enhance the profitability of the area, while gold occurrences, though less abundant, can supplement overall production. Ongoing exploration and resource assessments consistently confirm the Dyke's untapped potential, prompting continued investment in both large-scale operations and smaller ventures.

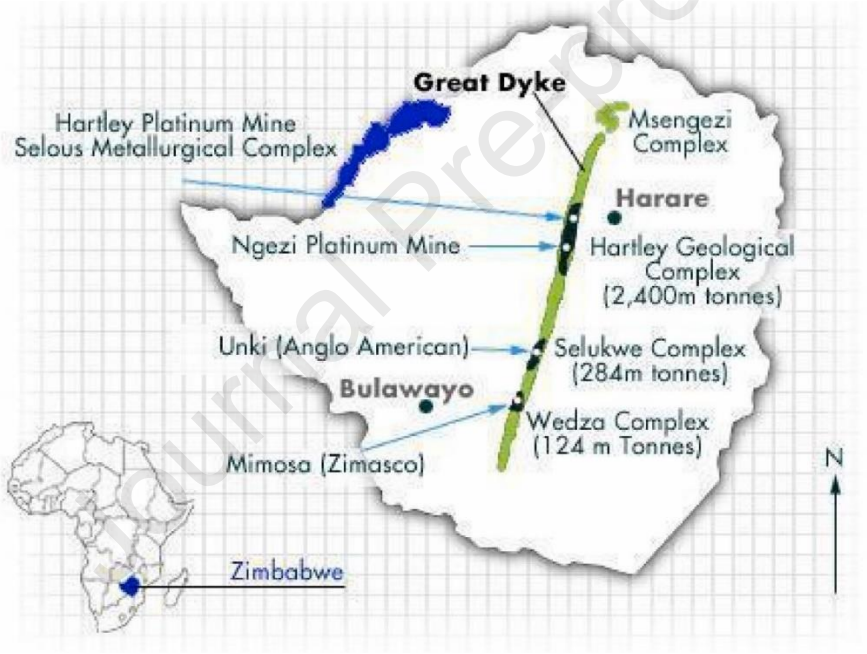

Figure 1. Great Dyke of Zimbabwe and its complexes (Siachingoma et al., 2023)

Figure 2 presents some of the geotechnical and geological challenges on the Great Dyke of Zimbabwe, calling for advanced robust approaches in rockmass characterisation for rock engineering designs.

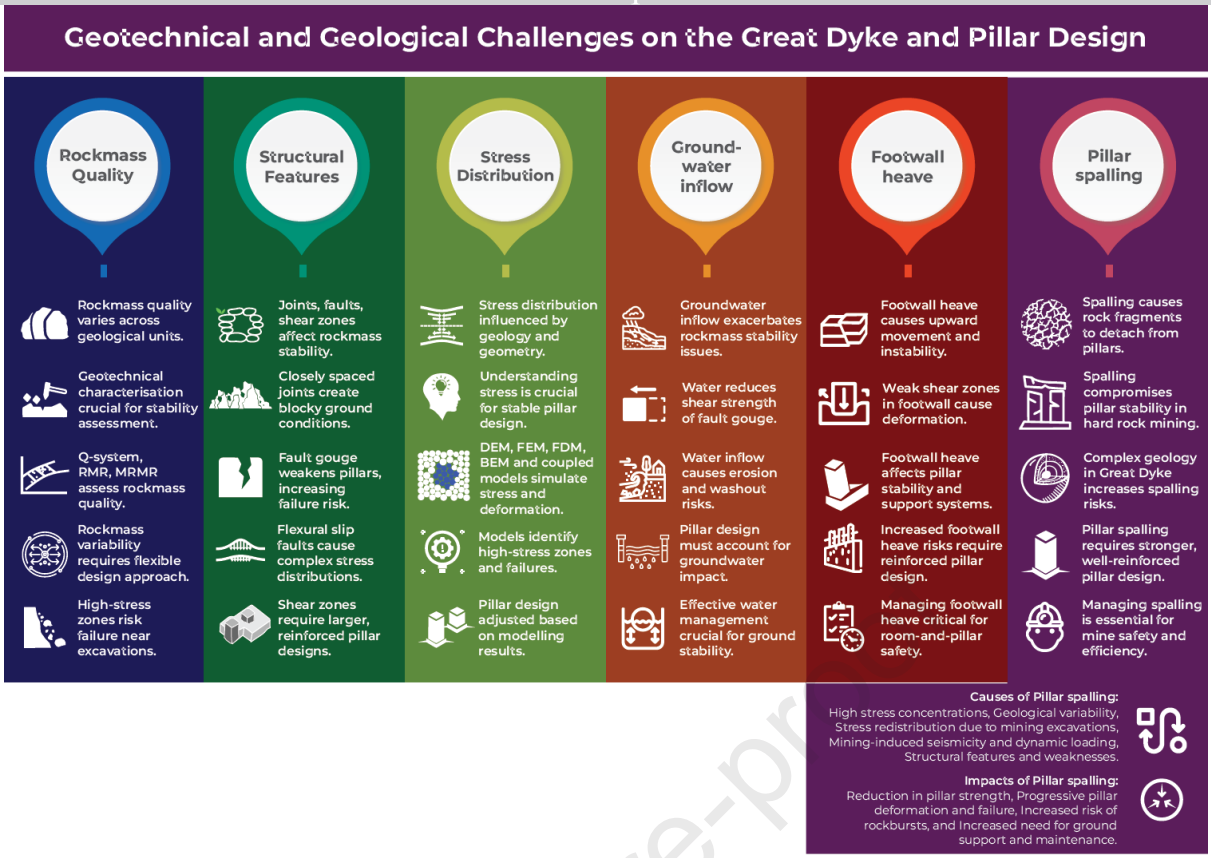

Figure 2. Geotechnical and geological challenges calling for advanced approaches in rockmass characterisation on the Great Dyke of Zimbabwe (Zvarivadza, 2025)

A previous separate extensive characterisation campaign from an exploration project shows the different geological and geotechnical challenges which exist on the Great Dyke of Zimbabwe. Figure 3 shows some observations from the exploration campaign.

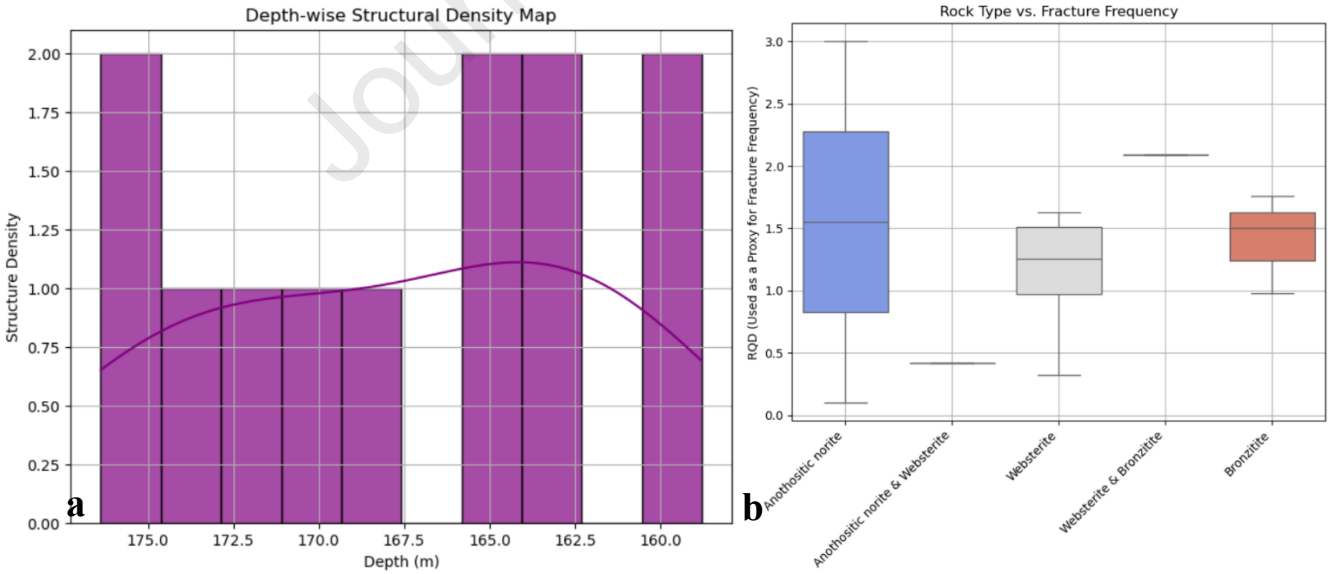

Figure 3. Great Dyke characterisation practical example a) depth-wise structural density, b) fracture distribution in relation to rock type

2.1 Site characterisation to determine Q-system and RMR-system parameters

Underground measurements (356 locations) were surveyed across the Wedza, Shurugwi, and Sebakwe subchambers of the Great Dyke of Zimbabwe, forming the foundation of both Q-system and RMR values used in this study. Since no drilling was performed, the determination of each parameter relied exclusively on in-situ observations, systematic geotechnical mapping, and laboratory tests on representative rock samples collected underground (rather than drill cores). This holistic approach ensured that all 356 pairs of Q and RMR values reflect genuine field conditions without the complexities of core recovery. To quantify the Q-system parameters, particular emphasis was placed on accurate joint mapping and rock structure assessment. For RQD, Palmström's (1982) formula (Eq. (3)) was adopted to circumvent the need for drillhole cores, relating RQD to the volumetric joint count J_v. The required input–average spacing of significant joint sets – was measured at each location. Specifically, three joint orientations were identified: strike-parallel joints (S_s), dip-related joints (S_d), and hanging wall joints (S_h). The volumetric joint count, J_v, emerged by summing the inverses of these three spacing values. Substituting J_v into Eq. (3), J_v yielded an RQD estimate, capped at 100% for computational consistency.

$$RQD = 115 - 3.3 \times J_v \quad (3)$$

The advantage of this method is its resilience to missing or incomplete core data – common in highly fractured or layered ultramafic rock—making it especially pertinent to the geological setting of the Great Dyke. After RQD was determined, the remaining Q-system parameters (J_n, J_r, J_a, J_w) were evaluated through direct inspection of pillars, backs (roof), and sidewalls. Observations included the count of joint families, the relative surface texture (ranging from very rough to polished), and any evidence of infilling, such as talc-chlorite seams or serpentinised coatings. Groundwater influences were classified by noting seepage intensity, seasonal inflow, and overall moisture conditions. For SRF, special consideration was given to in-situ stress conditions relative to the rock strength. Uniaxial Compressive Strength (UCS) values were determined using field Point Load Tests. Some underground rock samples were also taken for laboratory tests to corroborate measurements obtained from the Point Load Tests. The tests were conducted on intact rock samples obtained directly from existing faces or pillar failure remnants. These UCS results, coupled with visual indicators of stress damage – such as spalling or micro-fracturing–helped refine the SRF rating.

RMR was simultaneously evaluated at the same measurement points. Since RMR also requires RQD, the values derived from Palmström's formula were reused, ensuring consistency between the two classification schemes. The five additional RMR criteria parameters were addressed on-site as well. First, the intact rock strength, expressed primarily through UCS, was scored according to standard RMR tables. Next, the spacing of discontinuities was measured similarly to the Q-system approach, and discontinuity conditions–encompassing roughness, weathering, and infill thickness–were documented in parallel with J_r and J_a inspections. Groundwater conditions, likewise, were incorporated as a separate RMR component (slightly different in weighting from J_w). Finally, an orientation adjustment factor was applied if discontinuities were significantly oriented in a way that could promote instability, such as steeply dipping joints intersecting the roof or sidewall. Through the systematic collection of all Q-system and RMR parameters under actual underground conditions, this study avoids discrepancies that often arise when distinct data sources are used for different classification systems. The exclusive reliance on direct mapping and selective sampling also ensures that the 356 measurement points accurately represent the rock mass variability encountered in the ultramafic layers of the Great Dyke. Through this thorough approach, the resulting Q and RMR values reflect comprehensive, in-situ rock mass characteristics—offering a reliable dataset for subsequent analysis, design,

and predictive modelling efforts. Some of the rockmass characterisation locations for the project are shown in Fig. 4.

Figure 4. Practical field investigations: a) rockmass characterisation markings, b) structurally controlled slabbing and wedge failure

The descriptive statistic of the adopted dataset is presented in Table 2. The values of skewness and ketosis of the datasets point to the anti-normality of the data and are supported by the violin plots of the datasets in Fig. 5. The nature of the data distribution necessitates the use of advanced optimisation algorithm-based models as proposed in this study.

Table 2. Description of the datasets

								Skewness		Kurtosis	
	N	Missing	Mean	Median	SD	Minimum	Maximum	Skewness	SE	Kurtosis	SE
A	356	0	86.18	86.50	4.813	74.0	98.00	−0.0440	0.129	−0.75	0.258
B	356	0	11.37	12.00	2.413	3.0	15.00	−1.6755	0.129	3.36	0.258
C	356	0	1.42	1.50	0.578	1.0	9.00	6.9012	0.129	83.77	0.258

	N	Missing	Mean	Median	SD	Minimum	Maximum	Skewness		Kurtosis	
								Skewness	SE	Kurtosis	SE
D	356	0	2.95	2.00	1.273	1.0	6.00	1.0153	0.129	−0.01	0.258
E	356	0	1.01	1.00	0.175	0.5	3.00	5.1597	0.129	49.06	0.258
F	356	0	2.16	1.50	1.411	1.0	8.00	2.2385	0.129	4.79	0.258
G	356	0	50.52	51.10	3.504	36.0	59.43	−1.3786	0.129	3.50	0.258

A-RQD, B-J_n, C-J_r, D-J_a, E-J_w, F-SRF, G-RMR

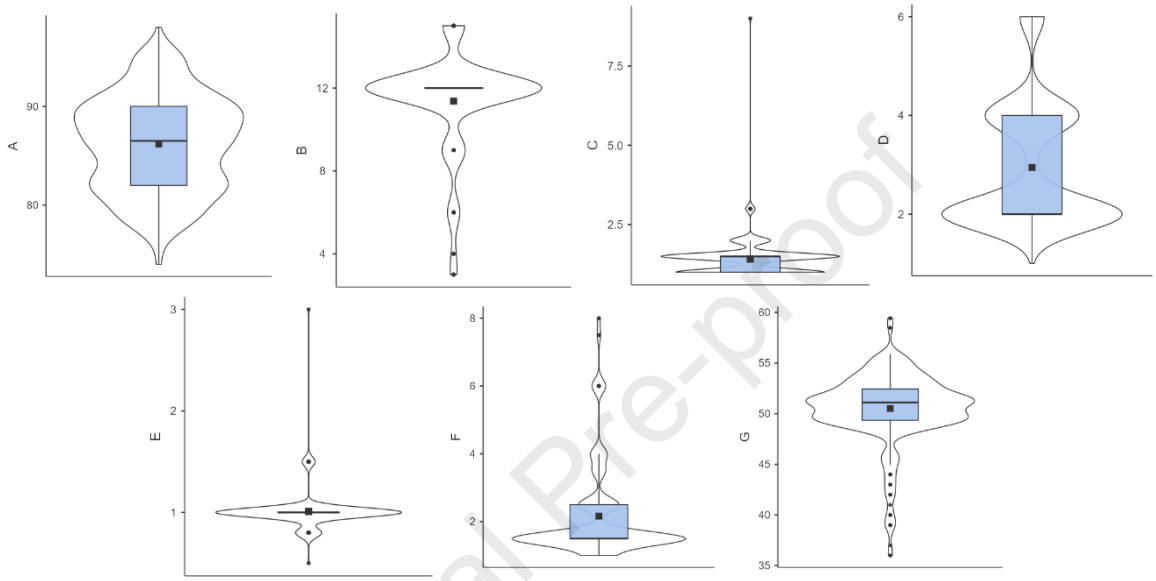

Figure 5. Violin plots of the model parameters

3 Model developments - optimisation algorithms

Optimisation algorithms are techniques used to find the best solution to a problem by either maximising or minimising an objective function. These algorithms are essential in fields like engineering, machine learning, finance, and operations research, as they help improve efficiency and performance. The brief description and implementation of the methods are presented as follows.

3.1 Flow Direction Optimisation Algorithm (FDA)

FDA is based on the principle of flow direction to the drainage point in the drainage basin with the lowest height. It was proposed by Karami et al. (2021) and it is adopted in this study to optimise the proposed ANN model for improved prediction of the RMR. The FDA mathematical formulation is based on the following assumptions:

- Individual flow has position and height.
- Around individual flow, there is a beta position with an objective function.
- There is a direct relationship between the flow speed and the slope.
- The flow moves in the direction with the lowest height with its speed *V*.
- The basin outlet point is the optimal flow location of the objective function.
- The following steps are essential in implementing the FDA algorithm.

1. Creating/generating the initial population or flows, which is depicted with the matrix in Eq. (4)

$$\mathrm{Flow_X} = \begin{bmatrix} \mathrm{x}_1^1 & \mathrm{x}_2^2 & \cdots & \mathrm{x}_d^1 \\ \mathrm{x}_1^2 & \mathrm{x}_2^2 & \cdots & \mathrm{x}_d^2 \\ \vdots & \vdots & \vdots & \vdots \\ \mathrm{x}_1^a & \mathrm{x}_2^a & \cdots & \mathrm{x}_d^a \end{bmatrix} \tag{4}$$

2. Objective function (OF) valuation and consideration of the best OF as the outlet point. The matrix of the OF is represented in Eq. (5)

$$\mathrm{Flow_{fitness}} = \begin{bmatrix} \mathrm{fitness}_1 \\ \mathrm{fitnesss}_2 \\ \vdots \\ \mathrm{fitnesss_a} \end{bmatrix} \tag{5}$$

3. Generating the quantities of neighbours (β) with neighbourhood radius delta (Eq. 6) for each individual of the population or flows

$$\Delta = \left(\mathrm{rand} * \mathrm{Xrand} - \mathrm{rand} * \mathrm{Flow_{X(}}_i\mathrm{)}\right) * \| \mathrm{Best_X} - \mathrm{Flow_{X(}}_i\mathrm{)} \| * \mathrm{W} \tag{6}$$

where rand depicts a random number with uniform distribution, Xrand is the random position while $\mathrm{Flow_{X(}}_i\mathrm{)}$ is the position of the flow (Eq. (7)) and W is the nonlinear weights with a random number between 0 and inf (Eq. (8)),

$$\mathrm{Flow_{X(}}_i\mathrm{)} = \mathrm{lb} + \mathrm{rand} * (\mathrm{ub} - \mathrm{lb}) \tag{7}$$

where ub and lb are the upper and lower limits of the decision variables respectively while rand depicts a random value between 0 and 1 with uniform distribution

$$\mathrm{W} = \left(\left(1 - \frac{\mathrm{iter}}{\mathrm{Max_{Iter}}}\right)^{2*\mathrm{randn}}\right) * \left(\overline{\mathrm{rand}} * \frac{\mathrm{iter}}{\mathrm{Max_{Iter}}}\right) * \overline{\mathrm{rand}} \tag{8}$$

4. Specifying the objective function value for each neighbour and determining the best neighbour

5. Step 6 should be implemented if the best neighbour has a better objective function than that of the current flow and if otherwise, step 7 is considered

6 Updating the flow velocity vector according to Eq. (9) and generating the new position of the flow based on Eq. (10).

$$V = \mathrm{randn} * \mathrm{S_0} \tag{9}$$

where $\mathrm{S_0}$ is given as:

$$\mathrm{S_0(i,j,d)} = \frac{\mathrm{Flow_{fitness(}}i\mathrm{)} - \mathrm{Neighbor_{fitness(}}j\mathrm{)}}{\|\mathrm{Flow_{x(}}i,d\mathrm{)} - \mathrm{Neighbor_{x(}}j,d\mathrm{)}\|} \tag{10}$$

where $\mathrm{Flow_{fitness(}}i\mathrm{)}$ and $\mathrm{Neighbour_{fitness(}}j\mathrm{)}$ are the respective objective values for the flow *i* and the neighbor *j*. The d parameter indicates the problem dimensions. The typical velocity vector of the flow is written as:

$$\mathrm{V} = [\mathrm{v}_1, \mathrm{v}_2, \ldots \mathrm{v}_d] \tag{11}$$

$$\mathrm{Flow_{newX(}}i\mathrm{)} = \mathrm{flow_{X(}}i\mathrm{)} + V * \frac{\mathrm{Flow_{X(}}i\mathrm{)} - \mathrm{Neighbor_{X(}}j\mathrm{)}}{\|\mathrm{Flow_{x(}}i\mathrm{)} - \mathrm{Neighbor_{x(}}j\mathrm{)}\|} \tag{12}$$

The $\mathrm{Neighbour_{X(}}j\mathrm{)}$ in Eq. (12) is given as

$$\text{Neighbour}_{X(j)} = \text{Flow}_{X(i)} + \text{randn} * \Delta \quad (13)$$

where $\text{Neighbour}_{X(j)}$ demonstrate the neighbour jth position and randn is a random value with normal distribution, zero mean and 1 standard deviation. The parameter Δ enables small and large numbers to search within the respective small and large ranges.

7. Updating the position of the flow using Eq. (14)

$$\begin{cases} \text{if } \text{Flow}_{\text{fitness}(r)} < \text{Flow}_{\text{fitness(i)}} \\ \text{Flow}_{\text{newX}(i)} = \text{Flow}_{X(i)} + \overline{\text{randn}} * \left(\text{Flow}_{X(r)} - \text{Flow}_{X(i)}\right) \\ \text{else} \\ \text{Flow}_{\text{newX}(i)} = \text{Flow}_{X(i)} + 2\text{randn} * \left(\text{Best}_X - \text{Flow}_{X(i)}\right) \\ \text{end} \end{cases} \quad (14)$$

8. Computing the objective function of new flows and updating the objective function and the position of the flows if it is better than the previous flows.

9. Controlling the terminate conditions; if it is met, return the optimal answer and if otherwise, repeat steps 3 and 7. The flowchart summarising the FDA algorithm is presented in Fig. 6.

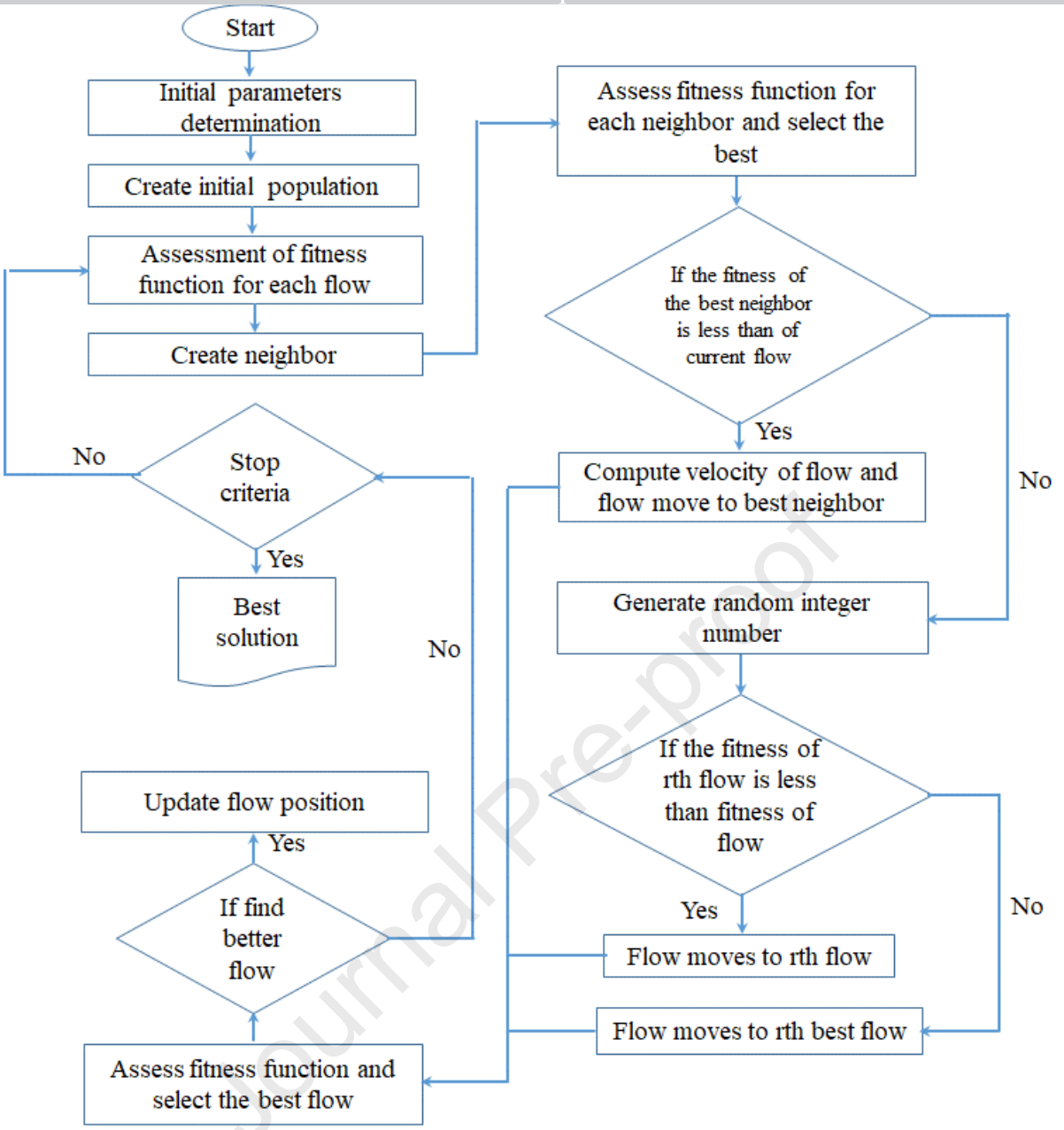

Figure 6. FDA flowchart (Son and Tri, 2024)

3.2 Sine-Cosine optimisation algorithm (SCA)

SCA proposed by (Mirjalili, 2016) belongs to the class of population-based algorithm inspired by the mathematical rules. SCA utilises the behaviour of mathematical functions which are sine and cosine for optimisation searching. Similar to many optimisation methods, there are also two optimisation phases in the SCA algorithm which are exploration and exploitation phases. The exploration phase combines random solutions with a high degree of randomness to locate the promising regions of the search space while there are changes in the random solutions with a lesser variation of the degree of randomness.

Mirjalili (2016) proposed Eqs. (15) and (16) for the position updating for the two phases.

$$X_i^{t+1} = X_i^t + r_1 \times \sin(r_2) \times \left| r_3 p_i^t - X_i^t \right| \quad (15)$$

$$X_i^{t+1} = X_i^t + r_1 \times \cos(r_2) \times \left| r_3 p_i^t - X_i^t \right| \quad (16)$$

where X_i^t is the position of the current solution in i-th dimension at t-th iteration, r_1 to r_3 are random numbers, and pi is the position of the destination point in i-th dimension. The combinations of Eqs. (15) and (16) can be expressed as in Eq. (17).

$$X_i^{t+1} = \begin{cases} X_i^t + r_1 \times \sin(r_2) \times \left| r_3 p_i^t - X_i^t \right|, & r_4 < 0.5 \\ X_i^t + r_1 \times \cos(r_2) \times \left| r_3 p_i^t - X_i^t \right|, & r_4 \geq 0.5 \end{cases} \quad (17)$$

The r_4 in Eq. (14) is a random number between 0 and 1. There are four fundamental parameters in SCA as presented in Eq. (17) which are r_1, r_2, r_3 and r_4. While r_1 determines the next position's region (Eq. (15)), r_2 expresses the extent of the movement towards or outwards the destination and r_3 gives a random weight for the destination to stochastically emphasise ($r_3 > 1$) or deemphasise ($r_3 < 1$) destination effect in expressing the distance. The switching between the sine and cosine components is achieved with r_4.

$$r_1 = a - t\frac{a}{T} \quad (18)$$

where t is the present iteration, T is the maximum iteration, and a is a constant. The flowchart for the implementation of SCA is presented in Fig. 7. The SCA is adopted in this study in addition to the FDA optimisation algorithm to optimise the ANN model proposed.

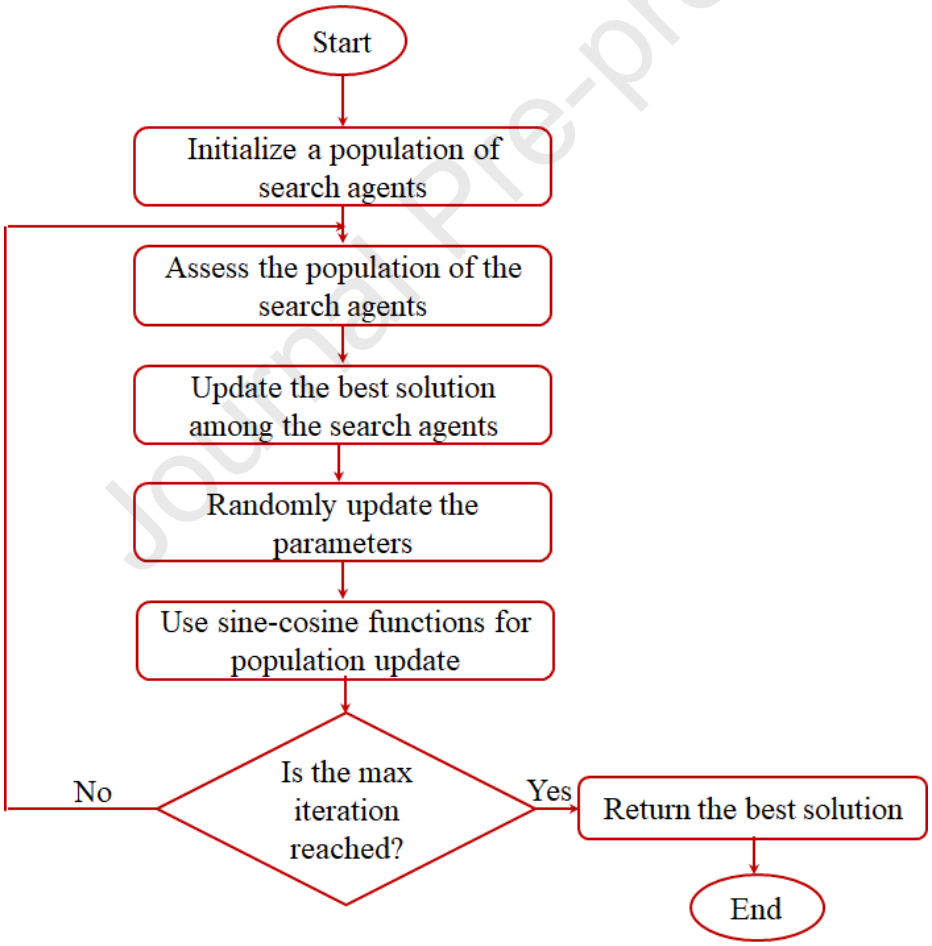

Figure 7. Original SCA flowchart (Rizk-Allah and Hassanien 2023)

3.3 Model implementation

The proposed ANN model in this study is a feed-forward neural network implemented in MATLAB software based on a backpropagation training algorithm sandwiched with the Levenberge Marquardt training function. The transfer function used between the first and

second layers for the single hidden layer type is hyperbolic tangent while for the double hidden layers, the purelin transfer function is deployed between the 2nd hidden layer and the output layer. Twelve different ANN architectures are simulated for the single hidden layer type (Table 3). Afterwards, the 6-10-1 ANN structure is selected as its testing case is slightly better than the 6-12-1 structure and an additional hidden layer is added to enhance the performance. For this case, the 6-10-15-1 network gives better performance than the other simulated ANN structures tried.

Table 3. Simulated ANN models

	Training	**Testing**	**Validation**	**Overall**
6-2-1	0.9501	0.98649	0.99212	0.96809
6-3-1	0.98852	0.98058	0.98704	0.98683
6-4-1	0.99078	0.99315	0.99318	0.99134
6-5-1	0.99557	0.98774	0.79929	0.95954
6-6-1	0.94409	0.99831	0.99669	0.96133
6-7-1	0.99682	0.99722	0.99696	0.99688
6-8-1	0.99587	0.9971	0.99901	0.99652
6-9-1	0.99693	0.98317	0.9985	0.99629
6-10-1	0.99654	0.9994	0.99689	0.997
6-11-1	0.99573	0.9991	0.99885	0.99697
6-12-1	0.99732	0.9993	0.99733	0.99757
6-13-1	0.95205	0.99554	0.99386	0.96189
6-10-10-1	0.99773	0.99751	0.9978	0.99767
6-10-15-1	0.9975	0.99973	0.9906	0.99774
6-10-20-3	0.99779	0.99123	0.99974	0.99772
6-10-25-1	0.99704	0.99313	0.9957	0.99657

For possible performance improvement, the 6-10-15-1 ANN structure is subjected to the optimisation algorithm using SCA and FDA which are yet to be used in optimising ANN in RMR prediction. Following the procedure presented previously, and by leveraging on the MATLAB code provided by Karami et al. (2021) for the FDA model and by Mirjalili (2016) for the SCA model, the FDA-ANN and SCA-ANN are developed. For the FDA optimisation algorithm, alpha and beta are set to 50 and 1 respectively with maximum iteration set to 500. For the SCA, the search agent is set to 200 while the iteration is set to 1000. The respective convergence curves for the FDA and SCA are presented in Figure 8 while the overall performances of the ANN, FDA-ANN and SCA-ANN are presented in Figures 9 to 11. The RMSE has reduced from 0.02005 to 0.01996 for SCA and 0.01878 for the FDA optimisation algorithm. The R values have also been consequently increased from 0.99774 to 0.99777 for SCA and to 0.99802 for the FDA-optimised ANN. More detailed evaluations of the proposed models using statistical indicators are presented in the next section.

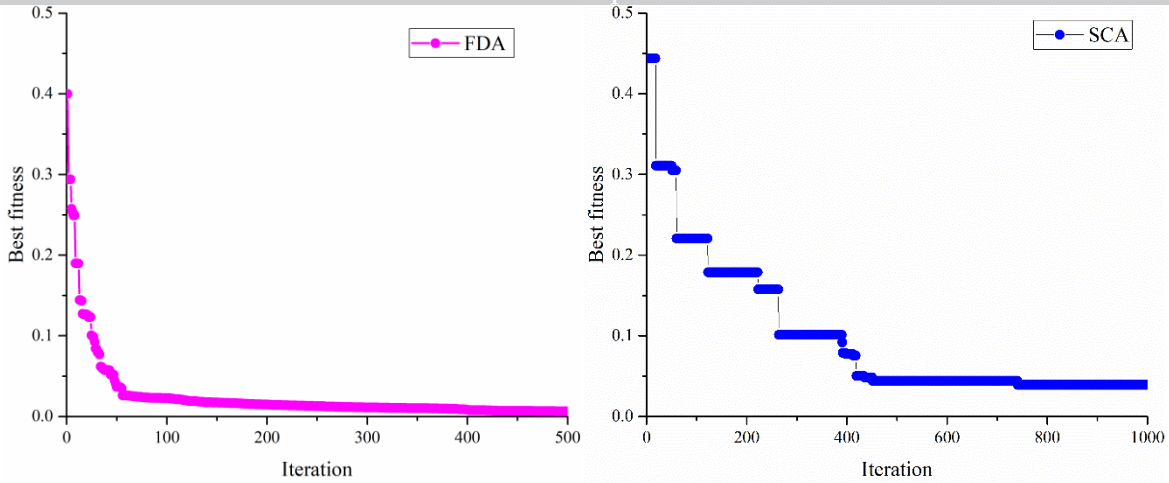

Figure 8. Convergence curves for (a) FDA and (b) SCA optimisation algorithms

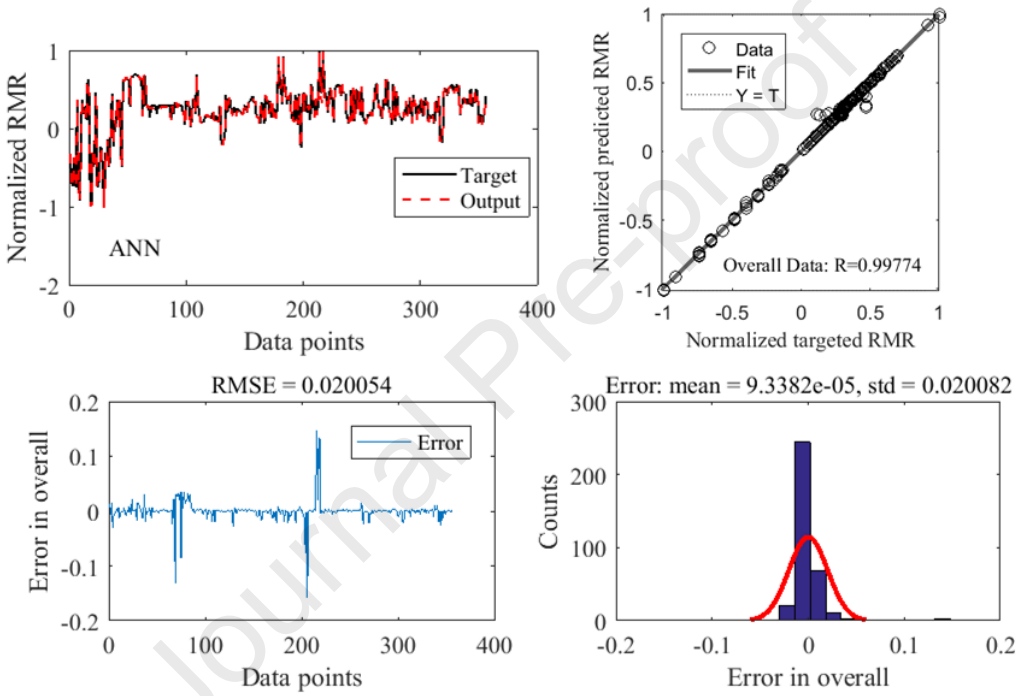

Figure 9. The normalised performance of the ANN model for the whole datasets

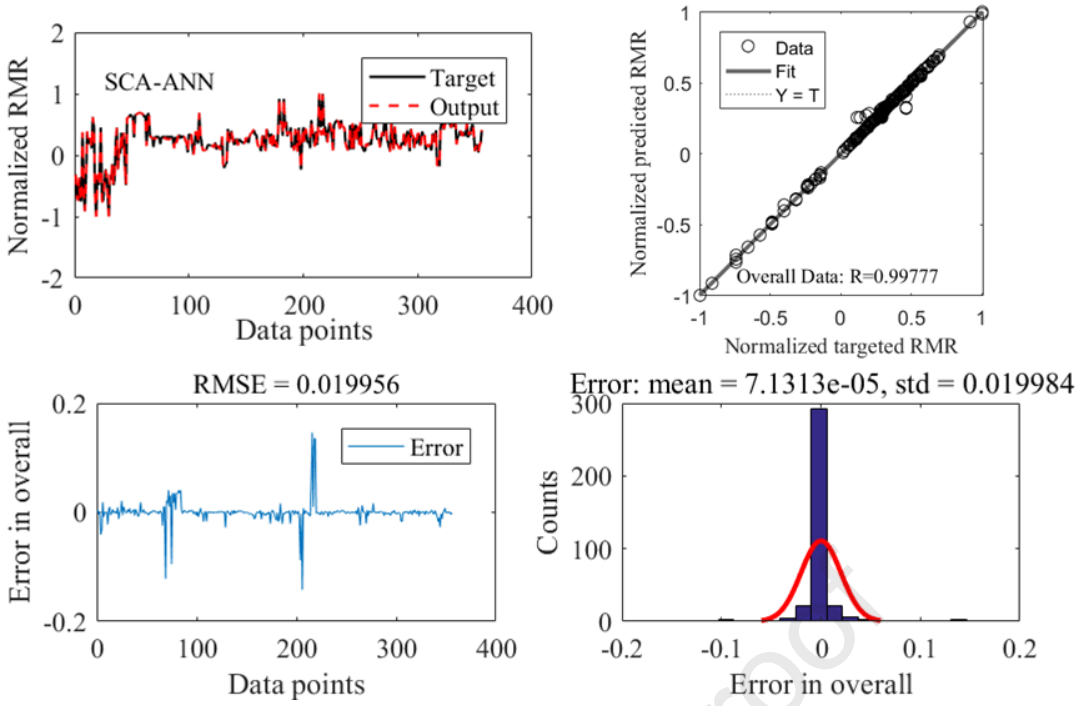

Figure 10. The normalised performance of the FDA-ANN model for the whole datasets

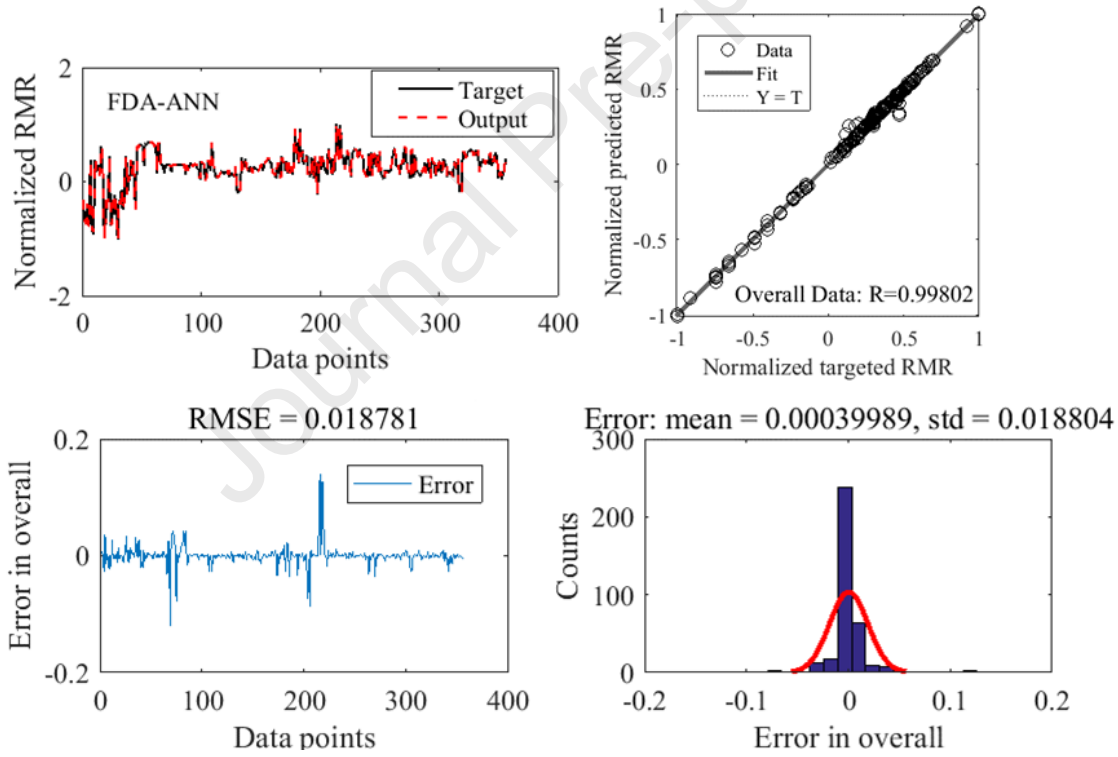

Figure 11. The normalised performance of the SCA-ANN model for the whole datasets

3.4 Model Performance Evaluation

The performance of the proposed ANN-based models is evaluated using statistical indicators such as coefficient of determination (R^2), root mean square error (RMSE), mean absolute error (MAE), mean absolute percentage error (MAPE), variance accounted for (VAF), Nash-Sutcliffe efficiency (NS), index of scatter (IOS), performance index (PI) and normalise mean bias error (NMBE) presented in Eqs. (19) to (27) as adopted in many of the existing studies.

$$R^2 = 1 - \frac{\sum_{i=1}^{r}(y_i - \bar{y})^2 - \sum_{i=1}^{r}(y_i - \hat{y}_i)^2}{\sum_{i=1}^{r}(y_i - \bar{y})^2} \tag{19}$$

$$\mathrm{RMSE} = \sqrt{\frac{1}{r}\sum_{i=1}^{r}(y_i - \hat{y}_i)^2} \tag{20}$$

$$\mathrm{MAE} = \frac{1}{r}\sum_{i=1}^{r}|y_i - \hat{y}_i| \tag{21}$$

$$\mathrm{MAPE} = \frac{1}{r}\sum_{i=1}^{r}\left|\frac{y_i - \hat{y}_i}{y_i}\right| \times 100\% \tag{22}$$

$$\mathrm{VAF} = \left(1 - \frac{\mathrm{var}(y_i - \hat{y}_i)}{\mathrm{var}(y_i)}\right) \times 100\% \tag{23}$$

$$\mathrm{NS} = 1 - \frac{\sum_{i=1}^{r}(y_i - \hat{y}_i)^2}{\sum_{i=1}^{r}(y_i - \bar{y})^2} \tag{24}$$

$$\mathrm{IOS} = \frac{\mathrm{RMSE}}{\bar{y}} \tag{25}$$

$$\mathrm{PI} = \mathrm{R}^2 + \left({}^{\mathrm{VAF}}/_{100}\right) - \mathrm{RMSE} \tag{26}$$

$$\mathrm{NMBE} = \frac{\frac{1}{r}\sum_{i=1}^{r}(\hat{y}_i - y_i)^2}{\frac{1}{r}\sum_{i=1}^{r}(y_i)^2} \tag{27}$$

where y_i is the actual value of the RMR, $\hat{y}_i$ is the predicted RMR, $\bar{y}$ is the mean of the actual RMR and r is the number of data points. The outcome of the evaluation based on these indices is presented in Table 4. The overall R^2 values for the ANN, FDA-ANN and SCA-ANN are 0.9951, 0.996 and 0.9955 respectively while their MAE values are 0.099, 0.096 and 0.085 for the respective ANN, FDA-ANN and SCA-ANN. The RMSE for the whole dataset for ANN is 0.244 and it is 0.22 for the FDA-ANN while that of the SCA-ANN is 0.23. The MAPE value for the ANN is 0.196 and for the FDA-ANN it is 0.192 while that of the SCA-ANN is 0.169. The VAF of 99.51 is obtained for the ANN while 99.6 and 99.55 are obtained for the FDA-ANN and SCA-ANN respectively. The NS values of 0.995, 0.996, and 0.9955 are obtained for the ANN, FDA-ANN and SCA-ANN models respectively. The ANN also has IOS of 0.0048 for the overall datasets while IOS of 0.0044 and 0.0046 are obtained for the FDA-ANN and SCA-ANN respectively. The PI of 1.746, 1.77 and 1.757 are respectively obtained for the ANN, FDA-ANN and SCA-ANN using the overall dataset. For the NMBE, 0.0012, 0.00099 and 0.0011 are obtained for the ANN, FDA-ANN and SCA-ANN respectively. The error values obtained for each of the models are very close to their expected value of 0 while their obtained R^2 and VAF are also much closer to the targeted value of 1 and 100% respectively. The PI is also close to the expected value of 2. Hence, the three proposed models can be used in assessing the RMR.

Table 4. Performance evaluation of the models

	R^2	MAE	RMSE	MAPE	VAF	NS	IOS	PI	NMBE
ANN	0.9951	0.099239	0.244036	0.196141	99.51374	0.995136	0.004831	1.746202	0.001179
FDA-ANN	0.996	0.096123	0.220025	0.191571	99.60482	0.996046	0.004355	1.772023	0.000958
SCA-ANN	0.9955	0.085382	0.233786	0.168863	99.55365	0.995536	0.004628	1.757251	0.001082

In addition, the scoring system was used to further evaluate the statistical indicators and easy visualisation of the model performances. The statistical indicators presented in Table 4 are ranked from 1 to 3. The model with the least error value is ranked as number 1 while the model with the highest error value is ranked 3. In the case of R^2, VAF, and PI, the model with the highest value is ranked 1st while the one with the least value is ranked 3rd. The outcome of the scoring of the model is displayed in the Chord diagram in Fig. 12. The chord diagram is produced for easy visualisation of the models. The three models are displayed in the diagram in connection to the performance indicator. The model with the smallest arc which is FDA-ANN is the best followed by the SCA-ANN with the arc length that is next to that of the FDA-ANN and then the model with the longest arc is the ANN which gives the least performance.

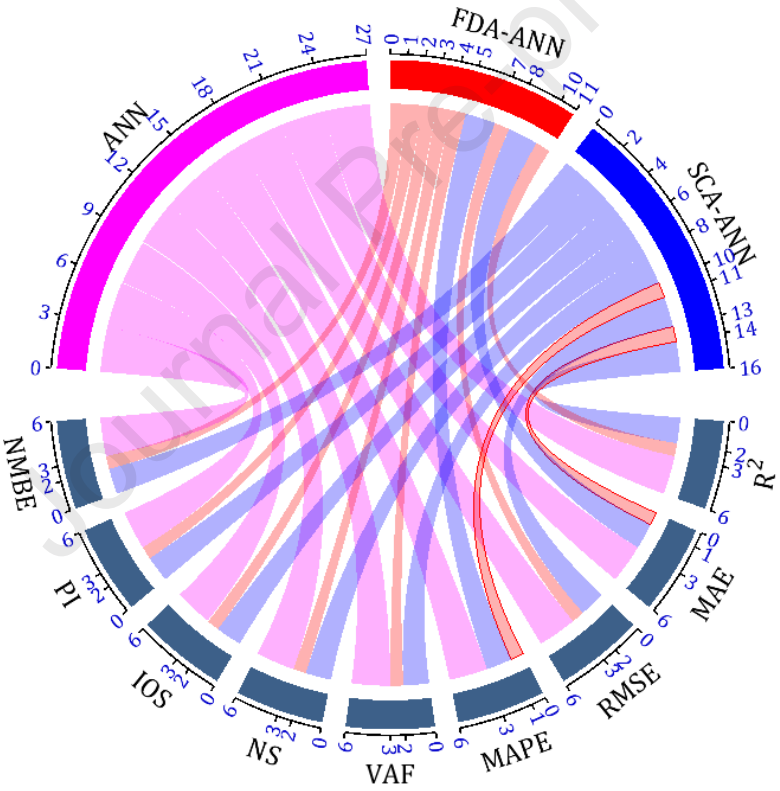

Figure 12. The scoring performance of the models

In comparison with existing studies on AI/ML prediction of RMR, Jalalifar et al. (2011) used ANFIS to predict the RMR using input parameters like UCS, RQD, Js, Jc and GW. The obtained R2 value for the best model among the three proposed ANFIS based on the subtractive clustering method is 0.964. Mutlu et al. (2017) used a defuzzification-free hierarchical fuzzy system to also predict the RMR using similar parameters as in the case of Jalalifar et al. (2011) and an R^2 of 0.897 is obtained. Most recently, Singh et al. (2025) predicted RMR using ANN, SVM and RF. The UCS was excluded from their model parameters. The r-value obtained for

the ANN is 0.92 (case 1) and 0.93 (case 2) while for the SVM, an r-value of 0.88 is obtained for case 1 and 0.95 for case 2 while for the RF model, 0.89 and 0.81 r values are obtained for the respective cases 1 and 2. In comparison with our proposed models, the performances of our proposed models are better as their R2 values exceed 0.99 which is better than most of the existing methods.

3.5 Sensitivity analysis

The sensitivity of the proposed model to the model parameters is conducted using the Cosine Amplitude methods as presented in Eq. (28). The method has been used to harness the sensitivity of the model features in various studies (Lawal et al. 2023; Onifade et al. 2024) and it is also used in this study due to its wide acceptance in machine learning/ soft computing studies. The expected value of CAM is 1 which implies that the model feature/parameter that is closer to or equal to 1 is the best influencing future. In this case, RQD has the highest CAM value followed by J_w and then J_n for all three models. CAM results are shown in Fig. 13.

$$\mathrm{CAM} = \frac{\sum_{k=1}^{m} \mathrm{input} \times \mathrm{target}}{\sqrt{\sum_{k=1}^{m} \mathrm{input}^2 \sum_{k=1}^{m} \mathrm{target}^2}} \tag{28}$$

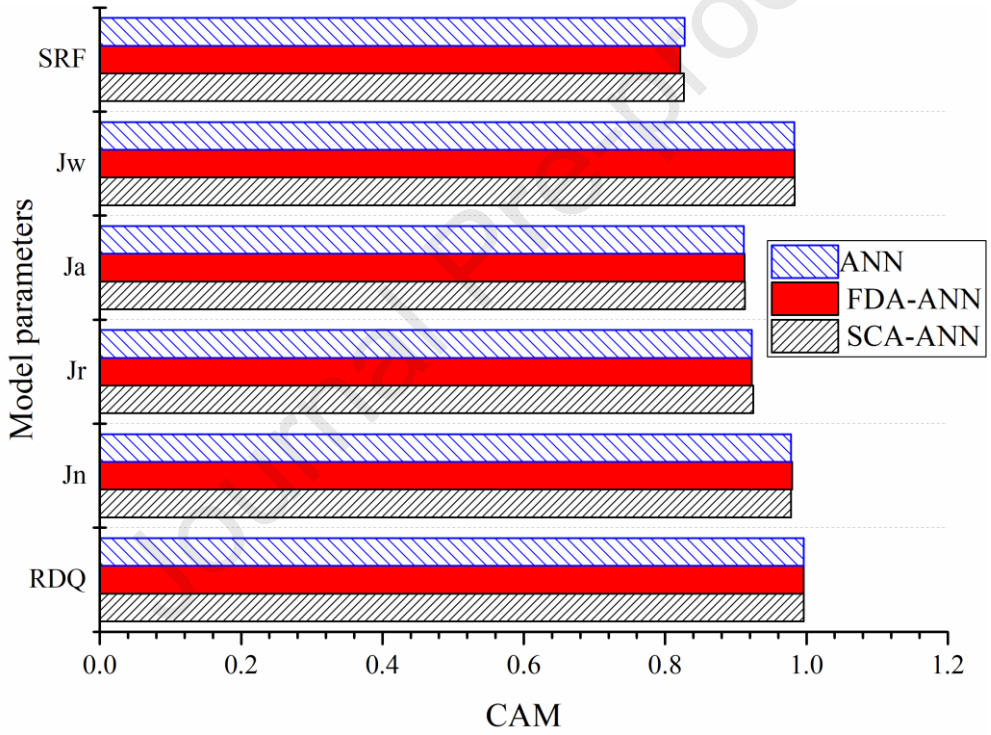

Figure 13. Relative importance of the model parameters

4 Conclusions

A crucial component of designing underground structures, support systems, stability analyses, and determining input parameters for numerical modelling within the rock mass environment are the rock mass classification systems, also referred to as empirical methods for rock mass classification. Based on the outcomes of rock mass characterisation, the empirical methods divide the rock masses into various groups with varying degrees of similar geological and geotechnical characteristics. Numerous rock mass classification systems were developed by various researchers based on their experiences and case studies in the fields of mining and civil engineering. To properly understand the classification of rock mass in the tunnelling face and lower the likelihood of disaster, this study adopted an advanced optimisation algorithm such as the novel Flow Direction optimisation Algorithm (FDA) and Sine-Cosine optimisation

algorithm (SCA) techniques to find the best solution considering the tunnel face's complexity and non-linearity.

A total number of 356 datasets with six rockmass parameters of the Q system (RQD, J_n, J_r, J_a, J_w, SRF) were used as input in this model while RMR was used as the output variable in this study. The performance of the proposed optimised ANN models is evaluated using the statistical indicators. The Chord diagram is used to rank the models and the CAM was used to determine the most pronounced parameters on RMR. The overall R^2 values for the ANN, FDA-ANN and SCA-ANN are 0.9951, 0.996 and 0.9955 respectively while their MAE values are 0.099, 0.096 and 0.085 for the respective ANN, FDA-ANN and SCA-ANN. The FDA-ANN model has a higher accuracy than other techniques, such as the ANN and SCA-ANN. The error values obtained for each of the models are very close to their expected value of 0 while their obtained R^2 and VAF are also much closer to the targeted value of 1 and 100% respectively. The PI is also close to the expected value of 2. Therefore, the three proposed models can be used in assessing the RMR using Q-parameters directly. This study provides a consistent and scalable method in addition to improving classification accuracy for RMR.

Author Contributions: Tawanda Zvarivadza: Conceptualisation, formal analysis, methodology, software, investigation, data curation, visualisation, writing–original draft preparation, writing–review and editing. **Abiodun Ismail Lawal**: Formal analysis, methodology, software, investigation, data curation, visualisation, writing–original draft preparation, writing–review and editing, supervision. **Moshood Onifade:** Formal analysis, methodology, investigation, resources, writing–original draft preparation, supervision. **Francois Mulenga**: Formal analysis, software, writing–review and editing, supervision. **Sangki Kwon**: Methodology, visualisation, writing and editing, supervision. **Manoj Khandelwal:** Conceptualisation, software, resources, writing–review and editing, supervision.

Data Availability: Data available from the corresponding author on request.

Competing interests: The authors declare no competing interests.

Acknowledgements: The authors would like to thank Rock Engineering practitioners who directly and indirectly contributed to the success of this research.

References

Abbas, N., Li, K.G., Emad, M.Z., Qin, Q., Li, M., Shah, K.S., Yue, R., Qiu, S., 2024. Empirical evaluation of RMR, GSI, and Q for underground excavations. Iranian Journal of Science and Technology, Transactions of Civil Engineering; 48(4), pp.2583–2594.

Adeli, H., 2001. Neural networks in civil engineering: 1989–2000. Computer-Aided Civil and Infrastructure Engineering; 16 (2), 126–142.

Aksoy, C.O., 2008 Review of rock mass rating classification: Historical developments, applications, and restrictions. Journal of Mining Science, 44, 51–63.

Armaghani, D.J., Mohamad, E.T., Narayanasamy, M.S., Narita, N., Yagiz, S., 2017. Development of hybrid intelligent models for predicting TBM penetration rate in hard rock condition. Tunnelling and Underground Space Technology, 63, 29–43.

Azarafza, M., Nanehkaran, Y.A., Rajabion, L., Akgün, H., Rahnamarad, J., Derakhshani, R., Raoof, A., 2020. Application of the modified Q-slope classification system for sedimentary rock slope stability assessment in Iran. Engineering Geology, 264, 105349.

Bao, H., Rao, Z., Lan, H., Yan, C., Liu, C., Liu, S., 2025. Discrete element modeling method for anisotropic mechanical behavior of biotite quartz schist based on mineral identification technology. Bulletin of Engineering Geology and the Environment, 84:28.

Bieniawski Z.T., 1976. Rock mass classification in rock engineering. In: Proceedings of the Symposium on Exploration for Rock Engineering. (Edited by Bieniawski Z.T.); Vol.1, pp. 97 –106. Cape Town, A.A. Balkema.

Bieniawski, Z.T., 1973 Engineering classification of jointed rock masses. Journal of the South African Institution of Civil Engineering, 15, 333–343.

Bieniawski, Z.T., 1989. Engineering Rock Mass Classification: A Complete Manual for Engineers and Geologists in Mining, Civil and Petroleum Engineering; John Wiley & Sons: Hoboken, NJ, USA, 1989.

Chen, J., Seo, H., Gao, C., Fang, Q., Zhang, D., Huang, H., 2024. A comprehensive method for similarity evaluation in discrete fracture network modeling of jointed rock masses. Rock Mechanics and Rock Engineering, 57(1), 639–653.

Chen, J., Yang, T., Zhang, D., Huang, H., Tian, Y., 2021. Deep learning-based classification of rock structure of tunnel face. Geoscience Frontiers, 12(1), 395–404.

Chen, L., Liu, Z., Su, H., Lin, F., Mao, W., 2022. Automated rock mass condition assessment during TBM tunnel excavation using deep learning. Scientific Reports, 12(1), 1722.

Choquet, P., Hadjigeorgiou, J., 1993. Design of Support for Underground Excavations, Chapter 12. In: Comprehensive Rock Engineering. J. Hudson (Ed.), Pergamon Press; Vol. 4, 314–348.

Deere, D.U., 1963. Technical description of rock cores for engineering purposes. Rock Mech. Engineering Geology, 1(1), 16–22.

Fathipour-Azar, H., 2021. Data-driven estimation of joint roughness coefficient. Journal of Rock Mechanics and Geotechnical Engineering, 13(6), 1428–1437.

Gao, Y.P., Li, X.Y., Gao, L., 2020. Discriminative stacked autoencoder for feature representation and classification. Science China Information Sciences, 63(2), 120111.

Gholami, R., Rasouli, V., Alimoradi, A., 2013. Improved RMR Rock Mass Classification Using Artificial Intelligence Algorithms. Rock Mechanics and Rock Engineering, 46, 1199–1209.

Han, S., Li, H., Li, M., Rose, T., 2019. A deep learning-based method for the nondestructive measuring of rock strength through hammering sound. Applied Sciences, 9(17), 3484.

He, M., Zhang, Z., Li, N., 2021. Deep convolutional neural network-based method for strength parameter prediction of jointed rock mass using drilling logging data. International Journal of Geomechanics, 21(7), 04021111.

Hochreiter, S., Schmidhuber, J., 1997. Long short-term memory. Neural Computation; Vol.9(8), 1735–1780,

Hoek, E., Kaiser, P.K., Bawden, W.F., 2000. Support of underground excavations in hard rock. CRC Press.

Holding, G., 2010. Training manual for production personnel in the principles of strata control. Great dyke geological succession.

Hou, S., Liu, Y., Yang, Q., 2022. Real-time prediction of rock mass classification based on TBM operation big data and stacking technique of ensemble learning. Journal of Rock Mechanics and Geotechnical Engineering, 14(1), 123–143.

Hu, J., Zhou, T., Ma, S., Yang, D., Guo, M., Huang, P., 2022. Rock mass classification prediction model using heuristic algorithms and support vector machines: a case study of Chambishi copper mine. Scientific Reports, 12(1), 928.

Hussain, S., Mohammad, N., Khan, M., Ur Rehman, Z., Tahir, M., 2016. Comparative Analysis of Rock Mass Rating Prediction Using Different Inductive Modelling Techniques. International Journal of Mining Engineering and Mineral Processing, 5(1), 9–15.

Jalalifar, H., Mojedifar, S. and Sahebi, A.A., 2014. Prediction of rock mass rating using fuzzy logic and multi-variable RMR regression model. International Journal of Mining Science and Technology, 24(2), 237–244.

Jin, C., Liang, J., Cui, J. and Wang, Q., 2023. Developing rock mass classification method using precise description of joints. Environmental Earth Sciences, 82(21), 487.

Karami, H., Anaraki, M.V., Farzin, S., Mirjalili, S., 2021. Flow direction algorithm (FDA): A novel optimization approach for solving optimisation problems. Computers & Industrial Engineering, 156, 107224.

Lawal, A. I., Hosseini, S., Kim, M., Ogunsola, N. O., Kwon, S., 2023. Prediction of factor of safety of slopes using stochastically modified ANN and classical methods: a rigorous statistical model selection approach. Natural Hazards. https://doi.org/10.1007/s11069-023-06275-5

Lawrence, S., Giles, C.L., Tsoi, A.C., Back, A.D., 1997. Face recognition: a convolutional neural-network approach. IEEE Trans. Neural Network, 8(1), 98–113.

Le Roux, N., Bengio, Y., 2008. Representational power of restricted Boltzmann machines and deep belief networks. Neural Computation, 20(6), 1631–1649.

Li, X., Chen, Z., Tang, L., Chen, C., Li, T., Ling, J., Lu, Y., Rui, Y., 2024. Predicting rock mass rating ahead of the tunnel face with Bayesian estimation. Frontiers in Earth Science, 12, 1333117.

Liu, C., Bao, H., Wang, T., Zhang, J., Lan, H., Qi, S., Wei Yuan, Shunichi Koshimura., 2025. Intelligent characterization of discontinuities and heterogeneity evaluation of potential hazard sources in high-steep rock slope by TLS-UAV technology; Journal of Rock Mechanics and Geotechnical Engineering. https://doi.org/10.1016/j.jrmge.2025.03.023.

Liu, C., Bao, H., Lan, H., Yan, C., Li., C., Liu., S., 2024.Failure evaluation and control factor analysis of slope block instability along traffic corridor in Southeastern Tibet. Journal of Mountain Science, 21(6): 1830–1848.

Liu, F., Liu, Y., Yang, T., Xin, J., Zhang, P., Dong, X., Zhang, H., 2021. Meticulous evaluation of rock mass quality in mine engineering based on machine learning of core photos. Chinese Journal of Geotechnical Engineering, 43(5), 968–974.

Mert, E., Yilmaz, S., İnal, M., 201. An assessment of total RMR classification system using unified simulation model based on artificial neural networks. Neural Computing and Applications, 20, 603–610.

Mirjalili, S., 2016. SCA: a sine cosine algorithm for solving optimisation problems. Knowledge-Based Systems, 96, 120–133.

Mutlu, B., Sezer, E.A., Nefeslioglu, H.A. A defuzzification-free hierarchical fuzzy system (DF-HFS): Rock mass rating prediction. Fuzzy Sets Syst. 307, 50–66.

Nejati, H.R., Ghazvinian, A., Moosavi, S.A., Sarfarazi, V., 2014. On the use of the RMR system for estimation of rock mass deformation modulus. Bulletin of engineering geology and the environment, 73, 531–540.

Narimani, S., Davarpanah, S.M., Bar, N., Vásárhelyi, B., 2025. Analyzing Drill Core Logging Using Rock Quality *Designation*–60 Years' Experience from Modifications to Applications. Applied Sciences; 15(3), 1309.

Onifade, M., Lawal, A.I., Bada, S.O., Khandelwa, M., 2024. Predictive modelling for coal abrasive index: Unveiling influential factors through Shallow and Deep Neural Networks. Fuel, 374, 132319.

Peng, Z., Su, P., Chen, W., Tao, H., Ma, G., Xia, Z. Bo, T., 2022. 3D quality evaluation of rock mass in urban underground space based on improved fuzzy analytic hierarchy process. KSCE Journal of Civil Engineering, 26(11), 4829–4839.

Ramamurthy, T., 1993. Strength and modulus responses of anisotropic rocks. Comprehensive rock engineering, 1(13), 313–329.

Rezaei, M., Habibi, H., 2023. Designing of the Beheshtabad water transmission tunnel based on the hybrid empirical method. Structural Engineering and Mechanics, 86(5), 621–633.

Rizk-Allah, R.M., Hassanien, A.E., 2023. A comprehensive survey on the sine–cosine optimisation algorithm. Artificial Intelligence Review, 56, 4801–4858.

Romana, M., 1985, September. New adjustment ratings for application of Bieniawski classification to slopes. In Proceedings of the international symposium on role of rock mechanics, Zacatecas, Mexico, 49–53.

Saadati, G., Javankhoshdel, S., Mohebbi Najm Abad, J., Mett, M., Kontrus, H., Schneider-Muntau, B., 2024. AI-powered geotechnics: enhancing rock mass classification for safer engineering practices. Rock Mechanics and Rock Engineering, 1–31.

Sadrossadat, E., Ghorbani, B., Oskooei, R., Kaboutari, M., 2018. Use of adaptive neuro-fuzzy inference system and gene expression programming methods for estimation of the bearing capacity of rock foundations. Engineering Computations, 35(5), 2078–2106.

Salimi, A., Rostami, J., Moormann, C., Hassanpour, J., 2018. Examining feasibility of developing a rock mass classification for hard rock TBM application using non-linear regression, regression tree and generic programming. Geotechnical and Geological Engineering, 36, 1145–1159.

Santos, A.E.M., Lana, M.S., Pereira, T.M., 2022. Evaluation of machine learning methods for rock mass classification. Neural Computing and Applications, 34(6), 4633–4642.

Sari, M., Karpuz, C., Ayday, C., 2010. Estimating rock mass properties using Monte Carlo simulation: Ankara andesites. Computers & Geosciences, 36(7), 959–969.

Serafim, J.L., 1983. Consideration of the geomechanical classification of Bieniawski. In Proc. int. symp. on engineering geology and underground construction (Vol. 1, 33–44).

Sheng, D., Yu, J., Tan, F., Tong, D., Yan, T., Lv, J., 2023. Rock mass quality classification based on deep learning: A feasibility study for stacked autoencoders. Journal of Rock Mechanics and Geotechnical Engineering, 15, 1749–1758.

Siachingoma, B., Hlatywayo, D.J., Midzi, V., Mare, L., 2023. Geophysical mapping of the occurrence of platinum group elements in the main sulphide zone of the Great Dyke in Zimbabwe. Journal of African Earth Sciences, 202, 104857.

Singh, J., Pradhan, S.P., Singh, M.P., 2025. Application of machine learning tools in predicting basic rock mass rating of mountainous road cut slopes. J. Earth Syst. Sci. 134:52.

Son, P.V.H., Tri, B.N., 2024. Construction management multiple-objective trade-off problems using the flow direction algorithm (FDA). Asian Journal of Civil Engineering, 25, 3415–3429.

Soufi, A., Bahi, L., Ouadif, L., Kissai, J. E., 2018. Correlation between Rock mass rating, Q-system and Rock mass index based on field data. In MATEC Web of Conferences (Vol. 149, p. 02030). EDP Sciences.

Spross, J., Stille, H., Johansson, F., Palmstrom, A., 2019. Principles of Risk-Based Rock Engineering Design. Rock Mechanics and Rock Engineering, 53, 1129–1143.

Stille, H., Palmström, A., 2003. Classification as a tool in rock engineering. Tunnelling and underground space technology, 18(4), 331–345.

Terzaghi, K., 1946. Rock defects and loads on tunnel supports. In: Proctor, R.V., White, T.L. (Eds.), Rock Tunnelling with Steel Supports. Commercial Shearing and Stamping Company, Youngstown, USA, 17–99.

Wang, P., Wang, S., Zhu, C., Zhang, Z., 2020. Classification and extent determination of rock slope using deep learning. Geomechanics and Geophysics for Geo-Energy and Geo-Resources, 6(1), 33.

Wu, L.Z., Li, S.H., Zhang, M., Zhang, L.M., 2019. A new method for classifying rock mass quality based on MCS and TOPSIS. Environmental Earth Sciences, 78(6), 199.

Wu, Y., Wang, S., 2024, April. Drillability classification and identification for rock mass based on machine learning. In Journal of Physics: Conference Series (Vol. 2738, No. 1, p. 012001). IOP Publishing.

Wu, Z., Wei, R., Chu, Z., Liu, Q., 2021. Real-time rock mass condition prediction with TBM tunnelling big data using a novel rock machine mutual feedback perception method. Journal of Rock Mechanics and Geotechnical Engineering, 13(6), 1311–1325.

Xuzhen-He, G. N., Xu, H., Dai, S., 2024. Development of Rock Classification Systems: A Comprehensive Review with Emphasis on Artificial Intelligence Techniques. Engineering, 217–245.

Zhang, W., Chen, J., Wang, Q., Ma, D., Niu, C., Zhang, W., 2013. Investigation of RQD variation with scanline length and optimal threshold based on three-dimensional fracture network modelling. Science China Technological Sciences, 56(3), 739–748.

Zhang, W., Li, H., Han, L., Chen, L., Wang, L., 2022. Slope stability prediction using ensemble learning techniques: a case study in Yunyang County, Chongqing, China. Journal of Rock Mechanics and Geotechnical Engineering, 14(4), 1089–1099.

Zhang, W., Phoon, K.K., 2022. Editorial for advances and applications of deep learning and soft computing in geotechnical underground engineering. Journal of Rock Mechanics and Geotechnical Engineering, 14(3), 671–673.

Zhu, F. W., Dui, G. S., Ren, Q. W., 2011. A continuum model of jointed rock masses based on micromechanics and its integration algorithm. Science China Technological Sciences, 54, 581–590.

Zvarivadza, T., Grobler, H., Onifade, M., Khandelwal, M., 2025. Geological and geotechnical challenges on the Great Dyke of Zimbabwe and their impact on hardrock pillar design – Accepted for Journal of Deep Underground Science and Engineering, Online ISSN:2770–1328.

RESEARCH HIGHLIGHTS

- Developed a deep learning-based tool to predict RMR values from Q-system parameters, reducing the need for extensive fieldwork.
- Compared ANN, FDA-ANN, and SCA-ANN models, with FDA-ANN achieving the highest accuracy ($R^2 = 0.996$, MAE = 0.096).
- Used Chord diagrams for performance ranking and Cosine Amplitude Methods (CAM) for sensitivity analysis, identifying RQD, Jw, and Jn as the most influential parameters.
- Demonstrated that AI-driven models outperform traditional empirical equations in RMR estimation with high precision.
- Provides a reliable and efficient alternative for geotechnical engineers and researchers in rock mass classification.

Declaration of interests

☒ The authors declare that they have no known competing financial interests or personal relationships that could have appeared to influence the work reported in this paper.

☐ The authors declare the following financial interests/personal relationships which may be considered as potential competing interests: